# Shock-wave reflections over double-concave cylindrical reflectors

## V. Soni[1], A. Hadjadj[1,†], A. Chaudhuri[2] and G. Ben-Dor[3]

[1]Normandie University, INSA of Rouen, CNRS, CORIA, 76000 Rouen, France

[2]Department of Aerospace Engineering and Engineering Mechanics, San Diego State University,
San Diego, CA 92182, USA

[3]Department of Mechanical Engineering, Pearlstone Center for Aeronautical Engineering Studies,
Faculty of Engineering Sciences, Ben-Gurion University of Negev, Beer Sheva, Israel

Numerical simulations were conducted to understand the different wave configurations associated with the shock-wave reflections over double-concave cylindrical surfaces. The reflectors were generated computationally by changing different geometrical parameters, such as the radii of curvature and the initial wedge angles. The incident-shock-wave Mach number was varied such as to cover subsonic, transonic and supersonic regimes of the flows induced by the incident shock. The study revealed a number of interesting wave features starting from the early stage of the shock interaction and transition to transitioned regular reflection (TRR) over the first concave surface, followed by complex shock reflections over the second one. Two new shock bifurcations have been found over the second wedge reflector, depending on the velocity of the additional wave that appears during the TRR over the first wedge reflector. Unlike the first reflector, the transition from a single-triple-point wave configuration (STP) to a double-triple-point wave configuration (DTP) and back occurred several times on the second reflector, indicating that the flow was capable of retaining the memory of the past events over the entire process.

**Key words:** compressible flows, shock waves

## 1. Introduction

The inherent properties of the complex flow features resulting from the shock-wave reflections over various geometries are essential to solve real world problems, such as those encountered in aerospace propulsion systems, combustion, detonation and explosion, since these phenomena involve drastic changes both in pressure and temperature. Thus, it has intrigued researchers to carry out in-depth investigations of these flow features in the past several decades.

The shock reflection phenomenon dates back to the 19th century with the pioneering work of Mach (1878), where he discovered the regular and Mach reflection structures. However, no significant advancement was made until the eminent work of von Neumann (1963) in the 1940s. Later, Smith (1945) and White (1951) discovered two

† Email address for correspondence: hadjadj@coria.fr

new reflection structures, namely complex Mach reflection (CMR), which was later renamed to transitional Mach reflection (TMR) and double Mach reflection (DMR), extending the theory presented by von Neumann. Since then, a sizable amount of work has been done strengthening the insight into the shock reflection phenomena for steady, pseudo-steady and unsteady flows (Bryson & Gross 1961; Heilig 1969; Henderson & Lozzi 1975; Ben-Dor & Glass 1979; Ben-Dor 1980; Ben-Dor, Takayama & Kawauchi 1980; Hornung 1986; Ben-Dor 1987; Kaca 1988). Lately, pseudo-steady and unsteady flows in particular have been the focus of several studies such as that of a planar shock propagating over a reflector that exhibits various reflection patterns. In pseudo-steady flows, the angle of incidence remains constant as the shock advances over a reflector, thereby maintaining a linear trajectory of the triple point (TP) for a typical single Mach reflection (SMR). In contrast, the shock encounters a constant change of the angle of incidence in the case of unsteady flows. Hence, the transient flows involve different transition processes from one reflection structure to the other depending on the shape and size of the reflecting surface.

A comprehensive study on these flow features in steady, pseudo-steady and unsteady configurations is detailed in Ben-Dor's monograph (Ben-Dor 2007). In particular, the shock reflection off cylindrical concave surfaces has been an area of intense research (e.g. Itoh, Okazaki & Itaya (1981), Gvozdeva, Lagutov & Fokeev (1982), Takayama & Ben-Dor (1983), Takayama & Sasaki (1983), Ben-Dor & Takayama (1985), Izumi, Aso & Nishida (1994), Skews & Kleine (2007), Gruber (2012) and Shadloo, Hadjadj & Chaudhuri (2014)). While the earlier of these studies focused on the phenomenology of the reflection process, the later ones concentrated on shock focusing and the post-shock flow characteristics. Additionally, the viscous effects on the shock reflection for pseudo-steady flows have been examined experimentally by Hornung & Taylor (1982) and computationally by Drikakis *et al.* (1997) for unsteady flows. Later, Kleine *et al.* (2014) presented a careful analysis of the nonlinear behaviour of the irregular shock reflection patterns with respect to the Reynolds number.

Figure 1 highlights the shock reflection patterns on a cylindrical concave reflector, where the compression waves arising from the steepening of the concave wall angle form a kink in the incident shock ($I$), which later develops into a direct Mach reflection (DiMR) with a TP, i.e. a structure having three shock waves (incident ($I$), reflected ($r$) and Mach stem (MS)) and a contact discontinuity (slipstream (SL)) meeting at the TP. As the shock progresses, the DiMR turns into an inverse Mach reflection (InMR) in which the TP moves towards the reflecting surface. A transition from an InMR to a transitioned regular reflection (TRR) takes place when the TP collides with the reflecting surface. The TRR exhibits a new TP supported by an additional shock $d'$ (see Ben-Dor & Elperin 1991).

The shock reflection process over irregular geometries has gained attention in recent years, whereby Skews & Blitterswijk (2011) studied shock reflections off combined surfaces of convex cylindrical reflectors and a flat surface. Recently, Geva, Ram & Sadot (2013) and Ram, Geva & Sadot (2015) conducted an experimental study of shock-wave reflections over double circular reflectors of cylindrical concave and convex surfaces. In contrast, the shock reflection process over double straight wedges was analysed experimentally by Ben-Dor, Dewey & Takayama (1987) with different combinations of wedge angles and incident-shock-wave Mach numbers. Based on the foregoing literature review, the desire to expand the knowledge of the shock reflection phenomenon to the case of double-concave wedge reflectors, which to the best of the authors' knowledge has never been investigated before, becomes the motivation of the present study.
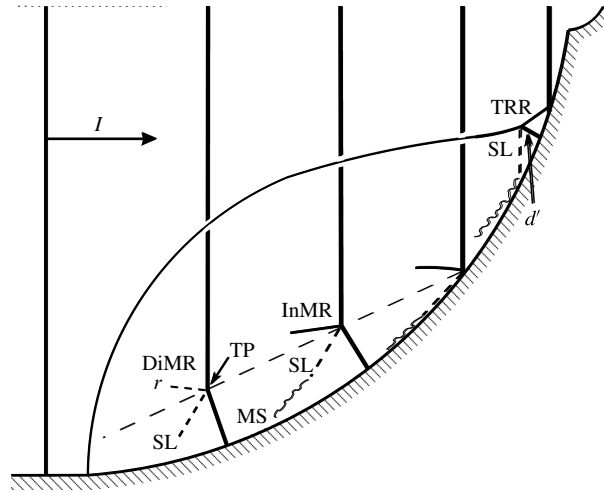
FIGURE 1. Schematic portrayal of the evolution of the shock-wave configurations over a concave cylindrical reflector. TP: triple point, *I*: incident shock, SL: slipstream, *r*: reflected shock, MS: Mach stem, *d′*: additional shock, DiMR: direct Mach reflection, InMR: inverse Mach reflection, TRR: transitioned regular reflection.

The shock reflection structures over single-concave reflectors are well known. The present study aims to improve our understanding of both weak and strong shock-waves reflection dynamics, specifically for the unsteady case of a propagating shock wave moving along double-concave wedge reflecting surfaces. From a fundamental viewpoint, having used the same concave cylindrical reflectors, it is believed that similar shock-wave reflection structures as observed on the first reflector would endure even on the second. However, the findings indicate that the reflection process over the second reflector differs considerably *vis-à-vis* the first one; and that it relies not only on the incident-shock-wave Mach number, but also on some of the other geometrical parameters of the reflectors. Moreover, a new shock-wave configuration transition cycle is discovered which passes as a single-triple point (STP) ↔ a double-triple point (DTP) several times on the same reflector. For further understanding, a series of numerical simulations have been performed with various incident-shock-wave Mach numbers, radii of the concave cylindrical surfaces and initial wedge angles. From a practical viewpoint, the usage of multiwedge reflectors may have several applications, such as to help better design new devices for high-speed combustion or detonation engines. One possible direct application for aeronautical and military industries is the pulsed and/or the rotating detonation engines (PDE or RDE) in which faster and well-controlled detonation ignition is highly desired.

## 2. Problem set-up

The computations were carried out using an in-house parallel compressible code equipped with the adaptive multiresolution method, which accounts for the space adaptivity for high CPU time and memory compression rates (Soni, Roussel & Hadjadj 2016). The code uses an immersed boundary method (IBM) to handle fluid–solid interaction problems (Chaudhuri, Hadjadj & Chinnayya 2011*a*). The solid body was localized inside a Cartesian grid using a ray tracing technique. For realistic
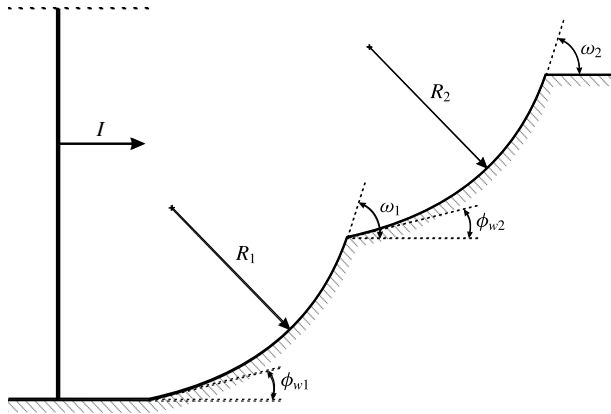
FIGURE 2. Schematic representation of a double-concave cylindrical reflector.

flow features, the Navier–Stokes equations coupled with the equation of state for an ideal gas and Sutherland's law were numerically solved. Here, the gas was considered as air with the ratio of heat capacities, $\gamma = 1.4$. Inviscid and viscous fluxes were computed using a fifth-order weighted essentially non-oscillatory (WENO) scheme and a fourth-order central difference formula, respectively, while the time was advanced using a third-order Runge–Kutta method (Chaudhuri *et al.* 2011*b*).

A schematic representation of the solid reflector is given in figure 2. As for the computational specifications, the boundary conditions were set to inlet and outlet at the left and the right of the computational domain, respectively, while a slip boundary condition was applied at the top boundary. Owing to the very short duration of the entire reflection process (240 μs for the slowest shock, $M_s = 1.2$ i.e. approximately 415 m s$^{-1}$, to pass the reflector), thermal effects, which take place on a much larger time scale, are negligibly small and can be ignored. Hence, the bottom surface was considered adiabatic with a no-slip boundary condition. The grid convergence studies were carried out by using different levels of grid refinement resulting in a variation of the first grid spacing in wall units $\Delta y_1^+$ from 40 to 8. However, for the phenomenological study of the shock-wave reflection structures, a good level of flow detail was found to be preserved by keeping $\Delta y_1^+ < 30$.

The study was divided into two parts.

 (i) Part I: analysis of the effect of the wedge angles of the cylindrical reflectors, $\phi_{w1} = \phi_{w2}$ on the shock reflection, when $R_1 = R_2 = 50$ mm, while $\omega_1 = \omega_2 = 75°$ were kept constant.
 (ii) Part II: analysis of the effect of the cylindrical surface radii, $R_1 = R_2$ on the reflection, when $\phi_{w1} = \phi_{w2} = 20°$, while $\omega_1 = \omega_2 = 75°$ were kept constant, and also the effect of the radius of the first cylindrical surface on the reflection, when $\phi_{w1} = \phi_{w2} = 0°$, $R_2 = 50$ mm, while $\omega_1 = \omega_2 = 75°$ were kept constant.

In all the simulations, the incident Mach number was varied in the range of $1.2 \leqslant M_s \leqslant 2.5$. Initially, the static pressure and temperature of the ambient conditions were taken as 101 325 Pa and 300 K, respectively, and the shocked-flow states were assigned using the Rankine–Hugoniot relations of a moving normal shock (Whitham 1999). As in Hadjadj & Kudryavtsev (2005), numerical schlieren pictures were used to highlight the different shock-wave structures.
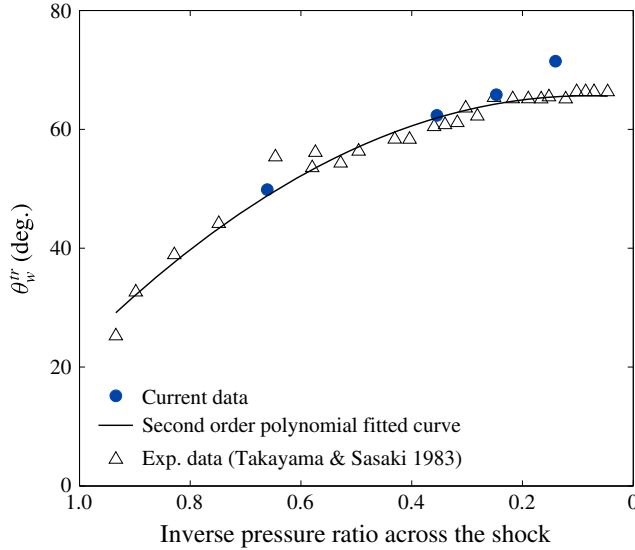
FIGURE 3. (Colour online) Comparison of numerical and experimental data for InMR $\rightarrow$ TRR transition angle on the first reflector using $R_1 = 50$ mm and $\phi_{w1} = 0°$ for various incident-shock-wave Mach numbers.

## 3. Validation of the numerical methodology

The numerical results obtained using the existing solver are validated against the experimental data to ensure the adequate reliability of the work. Since the numerical investigation presented here is altogether new, it is difficult to compare the entire flow configuration with a single experimental data set. Nevertheless, one of the geometrical combinations of the obstacles used is partially similar to that found in Takayama & Sasaki (1983). A comparison to the experimental data is made in terms of the transition angle, which can be defined as the angle formed at the point on the reflector, where the transition from the InMR to the TRR takes place. Numerically, it can be readily found by first obtaining the transition point from the triple-point trajectory, and then computing the slope of the line passing through it being tangential to the circular reflector. Figure 3 depicts a comparison of the current numerical model and the available experimental results (fitted with a second-order polynomial curve) for InMR $\rightarrow$ TRR transition angles on the first reflector of $R_1 = 50$ mm and $\phi_{w1} = 0°$. As can be seen, a quite good agreement has been found for the transition angles, except for $M_s = 2.5$ which exhibits an overestimation that could arise from a need for further local grid refinement near the critical points at high Mach numbers. Nevertheless, based on the current and past authors' results, one can consider that the overall methodology used in this study is able to ensure confidence in the accuracy of the simulations.

## 4. Results and discussion

### 4.1. *Part I: effect of the wedge angles* ($\phi_{w1} = \phi_{w2}$)

Four different wedge angles are considered, $\phi_{w1} = \phi_{w2} = 0°$, 10°, 20° and 30° with $M_s = 1.2$, 1.6, 1.9 and 2.5. In the case of $\phi_{w1} = \phi_{w2} = 0°$, the shock reflection patterns on the first concave reflector are similar to those reported in Ben-Dor (2007). Until the
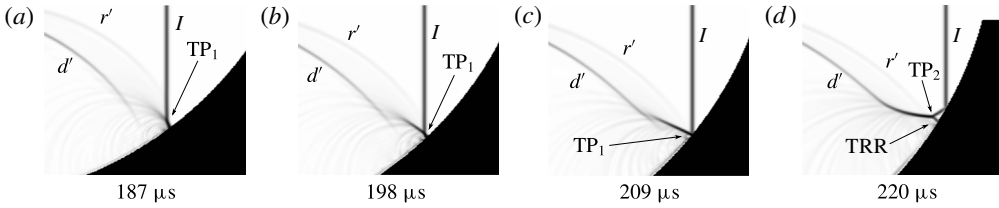
FIGURE 4. Numerical schlieren pictures for $M_s = 1.2$ and $\phi_{w1} = \phi_{w2} = 0°$ for the second concave surface. The origin of time is chosen such that the incident shock hits the inlet lip of the first reflector. $r'$ and $d'$: reflected and additional shocks created on the first reflector (TRR state), respectively, $I$: incident shock, TP: triple point.
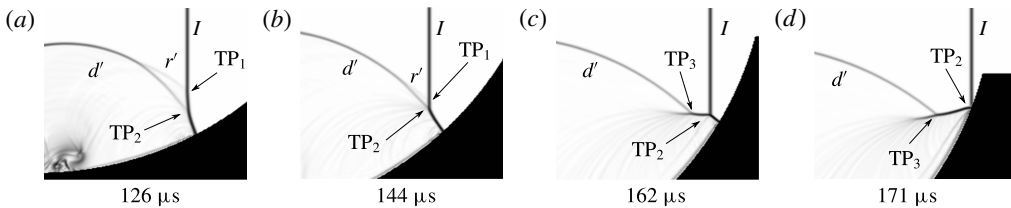


FIGURE 5. Numerical schlieren pictures for $M_s = 1.6$ and $\phi_{w1} = \phi_{w2} = 0°$ for the second concave surface. For legend, see caption of figure 4.

formation of $d'$ on the first reflector, the shock reflection phenomenon is fairly similar in all the considered cases with a slight variation in the computed InMR $\rightarrow$ TRR transition wedge angle, $\theta_w^{tr}$. However, as the incident shock wave propagates further and reaches the second concave reflector, the shock reflection pattern varies notably with both $M_s$ and $\phi_{w1}$. The following points describe the distinctive features with the different geometrical aspects over the second concave reflector:

$M_s = 1.2,\ \phi_{w1} = \phi_{w2} = 0°$

Figure 4 shows the shock reflection process on the second reflector, which closely resembles the one observed over the first reflector i.e. InMR $\rightarrow$ TRR (figure 4d). Although an additional wave, $d'$, reflected off the first surface (TRR), reaches the second reflector, it does not have enough velocity to catch up with the incident shock. Its influence on the entire process remains negligible, which makes the wave configurations similar to the ones observed over the first reflector i.e. an STP.

$M_s = 1.6,\ \phi_{w1} = \phi_{w2} = 0°$

When $M_s$ is increased to 1.6, before the additional shock wave, $d'$, reaches the incident shock, $I$, the reflected shock, $r'$, of the TRR over the first reflector forms a triple point (TP$_1$ in figure 5a) on the incident shock over the second reflector. The overall wave configuration is an STP. However, after being diffracted, $d'$ eventually catches up with $I$ (at its bottom) to form an additional TP (TP$_2$ in figure 5a). This makes a transition from a single-TP configuration to a double-TP configuration, which from here on will be referred to as STP and DTP, respectively. As $d'$ moves further up, the two triple points (TP$_1$ and TP$_2$) merge, and only TP$_2$ persists. As $I$ travels downstream, $d'$ starts falling behind, creating TP$_3$ (see figure 5c) followed by a transition to a TRR (not seen in figure 5). To the best of the authors' knowledge, this is the first time that the STP $\rightarrow$ DTP $\rightarrow$ STP $\rightarrow$ DTP overall wave configuration process has been observed
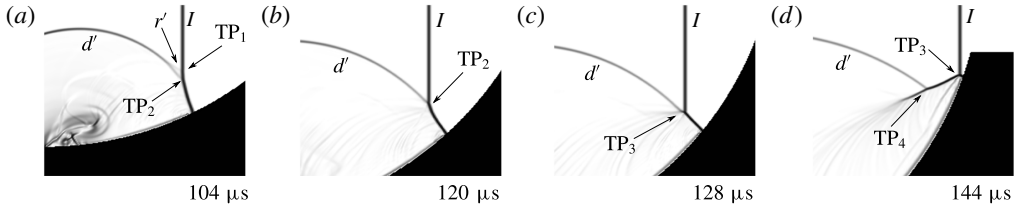
FIGURE 6. Numerical schlieren pictures for $M_s = 1.9$ and $\phi_{w1} = \phi_{w2} = 0°$ for the second concave surface. For legend, see caption of figure 4.
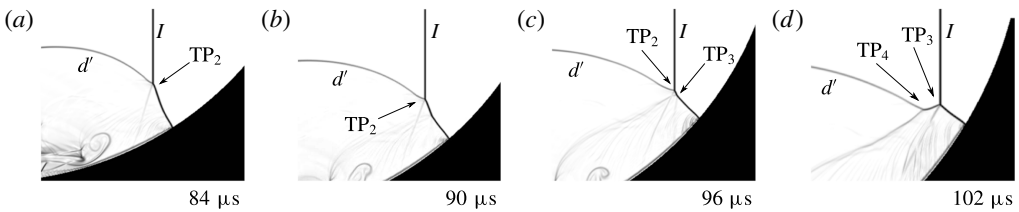


FIGURE 7. Numerical schlieren pictures for $M_s = 2.5$ and $\phi_{w1} = \phi_{w2} = 0°$ for the second concave surface. For legend, see caption of figure 4.

over the same reflector. This aspect is also highlighted by the triple-point trajectories that are shown in figure 11(b).

$M_s = 1.9$, $\phi_{w1} = \phi_{w2} = 0°$

When $M_s$ is increased to 1.9, the shock reflection phenomenon on the second reflector is similar to what has been observed in the case of $M_s = 1.6$. However, the length of the Mach stem associated with TP$_2$ (figure 6a) formed with the diffracted shock, $d'$, is quite substantial. This can be explained by the fact that with larger $M_s$, $d'$ moves vertically with higher velocity, which increases rapidly the height of the Mach stem over the reflector. Furthermore, as $I$ moves forward, the Mach stem starts to bend inwards, until it develops a kink and a new TP (TP$_3$ initiated between figure 6b,c) is formed and the overall reflection is DTP. Further up the reflecting surface, the two TPs merge to result in an STP wave configuration (figure 6c). Later on, the two TPs split to from a DTP wave configuration (TP$_3$ and TP$_4$ in figure 6d). Hence, the overall shock reflection cycle on the second reflector is STP $\leftrightarrow$ DTP for three times (see figure 11c).

$M_s = 2.5$, $\phi_{w1} = \phi_{w2} = 0°$

Rather complex wave configurations occur when $M_s$ is increased to 2.5 for which, unlike the previous cases, the incident-shock-induced flow is supersonic (the critical Mach number being $M_s^{crit} = 2.068$). The diffracted shock wave, $d'$, catches up with the incident shock right at the beginning of the second reflector. The SMR depicts a large Mach stem with a TP$_2$. As observed in the case of $M_s = 1.9$, it bends inward with time. However, the Mach stem curvature becomes significantly sharp until a new TP$_3$ (figure 7c) is developed, forming thereby an overall DTP wave configuration. This is a similar shock reflection behaviour to that observed by Colella & Glaz (1984) in the Mach stem of DMR for the hypersonic flow of $M_s = 8$ over an inclined ramp using a polytropic gas. As the shock proceeds further, the distance between the two TPs
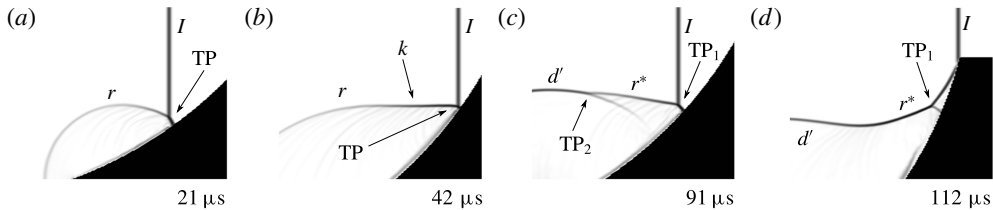
FIGURE 8. Numerical schlieren pictures for $M_s = 1.6$ and $\phi_{w1} = \phi_{w2} = 20°$ for (a,b) the first; and (c,d) the second concave surface. r: reflected shock on the first reflector (SMR state), I: incident shock, TP: triple point, k: reversal of curvature or kink (TMR state), d': additional shock created on the first reflector (TRR state), r*: reflected shock on the second reflector (SMR state).
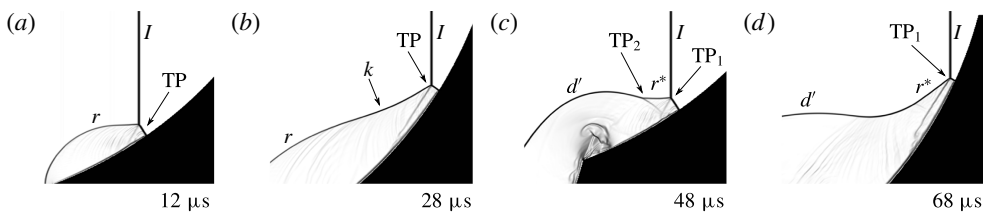


FIGURE 9. Numerical schlieren pictures for $M_s = 2.5$ and $\phi_{w1} = \phi_{w2} = 20°$ for (a,b) the first; and (c,d) the second concave surface. For legend, see caption of figure 8.

decreases as d' cannot reach I laterally. This leads to the momentary merger of the TPs (the slipstreams and the reflected shocks meet at a single point frame). Once d' falls behind I, a $TP_4$ appears (figure 7d). Therefore, similar shock reflection behaviour is observed on the second reflector as $M_s = 1.9$.

$M_s = 1.6$, $\phi_{w1} = \phi_{w2} = 20°$

With an initial wedge angle of $20°$, the shock reflection structure becomes a clear single Mach reflection over the first concave reflector from the very beginning (figure 8a). A clear transitional Mach reflection appears with a slight reversal of curvature, which could develop to a kink, k, visible on the reflected wave structure (figure 8b). Upon the TP impingement on the reflector surface, the wave configuration becomes a TRR, before I reaches the second reflector. But, as soon as I reaches it, an SMR with $TP_1$ appears. After getting diffracted, d' penetrates the reflected wave, r*, of $TP_1$ on the second reflector (figure 8c). This configuration resembles a typical DMR without a visible second slipstream that should emanate from $TP_2$. As I propagates further, a transition to TRR takes place. One can see that as it merges with d', the curvature in r* of the TRR is enhanced. Note that this makes an STP $\rightarrow$ DTP $\rightarrow$ STP transition process.

$M_s = 2.5$, $\phi_{w1} = \phi_{w2} = 20°$

As shown in figure 9(a,b), the shock reflection configurations are similar to the ones reported on the first concave reflector for $M_s = 1.6$ (figure 8a,b). However, the reversal of curvature or kink in TMR stands out distinctly in the current case (figure 9b). Over the second concave reflector, d' penetrates r* of SMR resembling a DMR without a visible second slipstream at $TP_2$. As I further progresses, interestingly, the DMR
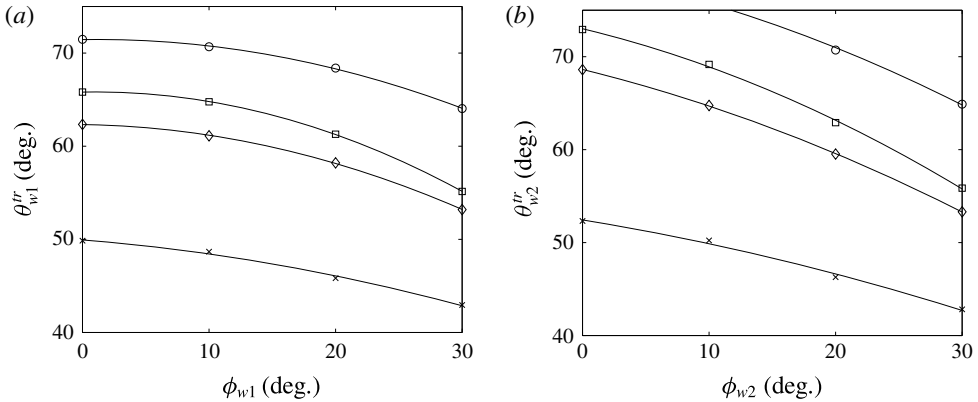
FIGURE 10. InMR → TRR transition angle over (*a*) the first; and (*b*) the second cylindrical concave reflector. By varying initial wedge angles $\phi_{w1} = \phi_{w2}$ for different incident-shock-wave Mach numbers, ○- $M_s = 2.5$, □- $M_s = 1.9$, ◇ $M_s = 1.6$, ×-$M_s = 1.2$.

transitions back to a TMR (figure 9*d*) followed by a TRR at the end (not shown in figure 9). In contrast to the past studies where the SMR → TMR → DMR transition process has been observed, here an SMR → DMR → TMR transition process is observed. To the best of the authors' knowledge this transition process has never been reported before.

Figure 10(*a,b*) shows the InMR → TRR transition angles, $\theta_w^{tr}$, over the first and the second reflectors. As can be seen, $\theta_w^{tr}$ increases for larger $M_s$. However, $\theta_w^{tr}$ decreases with the increase of the initial wedge angle $\phi_w$ over both reflectors. It is also interesting to note that even though both reflectors are identical, $\theta_w^{tr}$ is larger on the second one. This behaviour can be perceived as resulting from the fact that the flow regions behind the Mach stems are subsonic, hence the information can be communicated through them.

### 4.1.1. *Trajectories of the triple points*

In order to track the triple points, the $\ell^2$-norm of the pressure gradient is computed, which translates to the analytical formula for the two-dimensional case at the *n*th time step as,

$$\text{TP}_n = \sqrt{\left(\frac{\partial p}{\partial x}\right)_n^2 + \left(\frac{\partial p}{\partial y}\right)_n^2}. \tag{4.1}$$

Applying max($\text{TP}_n$, $\text{TP}_{n-1}$) for each time step would give the entire trajectories of the triple points. Figure 11 depicts the TP trajectories obtained for $\phi_{w1} = \phi_{w2} = 0°$ and 20°. Red-dashed lines show the formation of a weak Mach reflection (wMR) with the reflected shock wave carried forward from the TRR state over the first reflector. Conversely, blue-dashed lines represent the wMR being the second TP of a DMR developing from the diffracted shock. Notably, the shock-wave reflection phenomenon over the second cylindrical concave reflector depends on the additional shock of TRR, which is diffracted while leaving the first reflector. The velocity of the diffracted shock changes the shock reflection structures depending on the initial wedge angle and the incident-shock-wave Mach number.
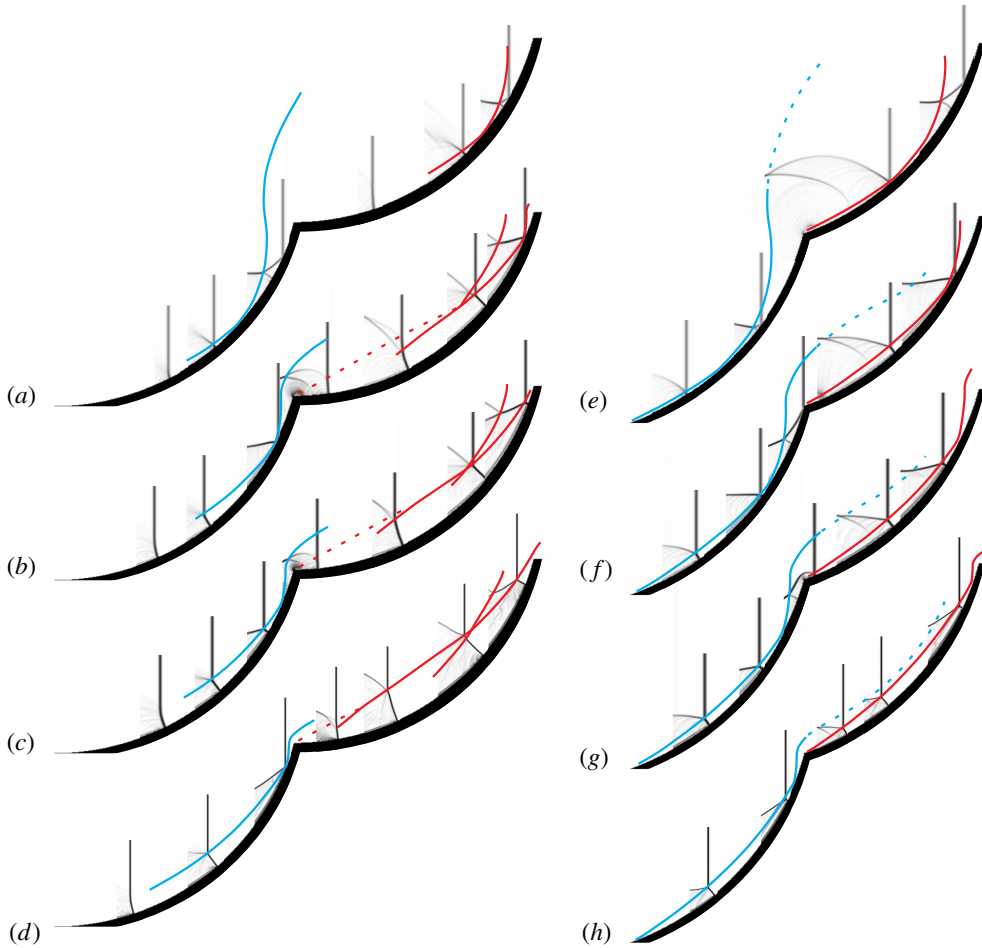
FIGURE 11. (Colour online) Trajectories of the triple points: (*a–d*) with $\phi_{w1} = \phi_{w2} = 0°$ for $M_s = 1.2$, 1.6, 1.9 and 2.5 in ascending order from top to bottom; (*e–h*) with $\phi_{w1} = \phi_{w2} = 20°$ for $M_s = 1.2$, 1.6, 1.9 and 2.5 in ascending order from top to bottom. The blue and red solid lines correspond to TP trajectories on the first and second reflectors, respectively; while the dashed line highlights the TP of the weak Mach reflection.

### 4.1.2. *Reflector junction effect*

The effect of the junction between the two reflectors over the shock reflection patterns on the second reflector is investigated by replacing the sharp corner with a continuous smooth radius of $R = 6$ mm. The models generated by doing so are presented in figure 12. The model A is created by adding a small cylindrical convex part, such that the convex surface begins at $\omega_1 = 75°$ and ends at $\phi_{w1} = 0°$, while the model B has a fillet curve of cylindrical convex, thereby reducing $\omega_1$ by $\delta$ and similarly increasing $\phi_{w2}$ by the same value.

Model A: $M_s = 2.5$, $\phi_{w1} = \phi_{w2} = 0°$

Since the first reflector is unchanged, the associated reflection remains exactly the same as reported previously. Figure 13(*a,b*) depicts the shock reflection in the vicinity of the corner. Unlike in the sharp corner case, no wMR is found on the
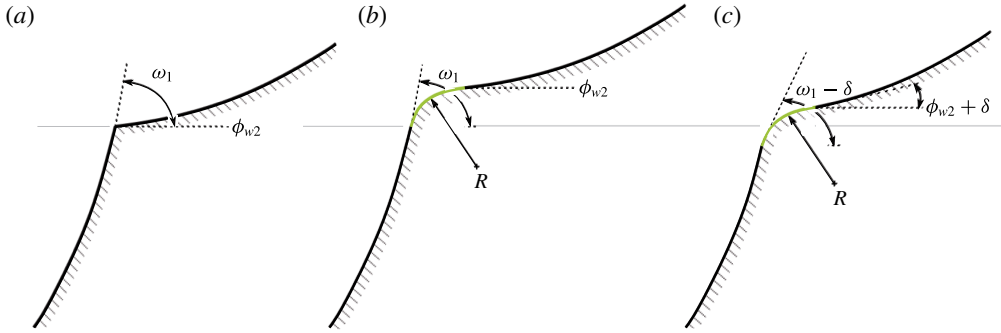
FIGURE 12. (Colour online) Schematic illustration of the three cases of the reflector junction: (*a*) sharp edge junction for $\omega_1 = 75°$ and $\phi_{w2} = 0°$; (*b*) model A where the geometrical parameters of the original geometry is preserved; and (*c*) model B in which the junction is replaced by a fillet curve of radius, $R = 6$ mm, and $\delta = 5.49°$.
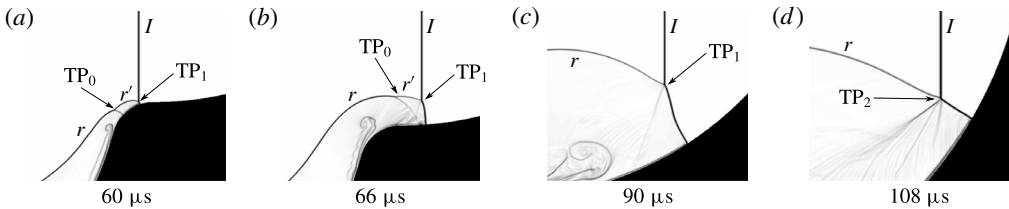


FIGURE 13. Numerical schlieren pictures for $M_s = 2.5$ and $\phi_{w1} = \phi_{w2} = 0°$ for model A showing the time evolution of the shock reflection (*a*,*b*) on/near the junction; and (*c*,*d*) on second concave surface. *r*: reflected shock on the first reflector (DiMR state), *I*: incident shock, TP: triple point, *r'*: reflected shock created on the first reflector (TRR state).

second reflector, as a result of a possible transition to MR ($TP_1$ and *r'*) over the convex surface. The reflection structure of DTP (with $TP_0$ and $TP_1$ in figure 13*b*) is transitioned to STP (with $TP_1$ see figure 13*c*). This Mach stem bends inwards and develops a kink emanating a slipstream ($TP_2$) from it, which merges with $TP_1$ (see figure 13*d*). Hence, from figure 13(*c*) onwards the shock reflection patterns are identical to those of the sharp corner case (see figure 7*b*).

Model B: $M_s = 2.5$, $\phi_{w1} = 0°$ $\phi_{w2} = 0° + \delta$

Figure 14(*a*,*b*) highlights the reflection process in the proximity of the corner. As it can be seen, there is no clear transition from InMR → TRR, but rather InMR → RR → DiMR over the corner. This can be explained by the fact that by the time the TP reaches the reflecting wall, it falls on the cylindrical convex surface as a result of the reduction in $\omega_1$. Noticeably, since there is no TRR, there is no additional shock *d'* which could involve in the shock reflections on the second reflector. Nevertheless, STP (with $TP_1$ see figure 14*c*) on the second reflector has a large Mach stem, which, as it bends inwards, forms $TP_2$ (see figure 14*d*); and hence, the overall transition follows STP → DTP → STP → DTP. As it can be noticed, the shock reflection is substantially different compared to the model A. However, it is observed that for smaller Mach numbers, the shock reflection is identical to that observed for model A with a little change in InMR → TRR transition angle due to the additional distance added between the two reflectors in model A.
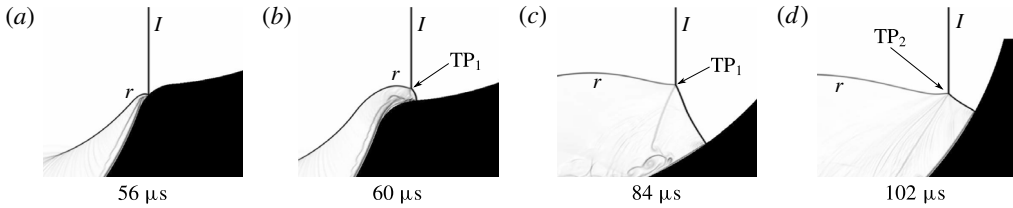
FIGURE 14. Numerical schlieren pictures for $M_s = 2.5$ and $\phi_{w1} = 0°$, $\phi_{w2} = 0° + \delta$ for model B showing the time evolution of the shock reflection (a,b) on/near the junction; and (c,d) on second concave surface. For legend, see caption of figure 13.
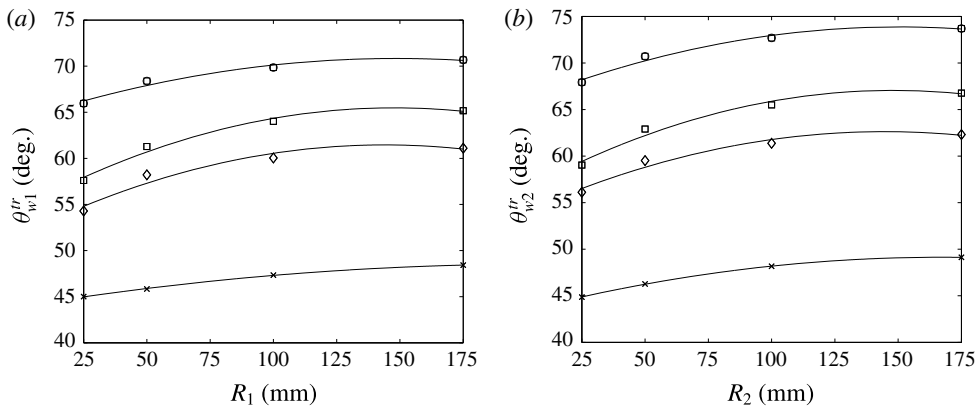


FIGURE 15. InMR $\rightarrow$ TRR transition angle over (a) the first; and (b) the second cylindrical concave reflector. By varying reflector radii, $R_1 = R_2$ for different incident-shock-wave Mach numbers, $\bigcirc$- $M_s = 2.5$, $\square$- $M_s = 1.9$, $\diamond$ $M_s = 1.6$, $\times$-$M_s = 1.2$.

## 4.2. *Part II: effect of the cylindrical surface radii*

In order to better understand the effect of radius on the shock reflection phenomenon over the second cylindrical concave reflector, numerical tests are conducted by varying the radius of both reflectors as $R_1 = R_2 = 25$, 50, 100 and 175 mm, while the initial wedge angles are kept constant as $\phi_{w1} = \phi_{w2} = 20°$ and $\omega_1 = \omega_2 = 75°$. It is found that for different incident-shock-wave Mach numbers, $M_s = 1.2$, 1.6, 1.9 and 2.5, apart from the change in the transition angle, no significant difference in the shock reflection patterns is observed.

The measured InMR $\rightarrow$ TRR transition angles on the first and on the second cylindrical reflectors are given in figures 15(a) and 15(b), respectively. The results show that the transition is delayed as $M_s$ increases. The same trend is observed when increasing the radius of curvature. Moreover, the difference between the transition angles on the first and second reflector gets bigger with larger $M_s$.

The effect of radius of the first cylindrical concave reflector is also investigated by varying $R_1 = 25$, 50, 100 and 175 mm for different $M_s$, while keeping $R_2 = 50$ mm and $\phi_{w1} = \phi_{w2} = 0°$. Although no new shock structures other than those reported in Part I are found, the radius of the first surface has a very dramatic effect on the shock reflection phenomenon over the second reflector. For the smaller radius, $R_1 = 25$ mm with $M_s = 1.2$, the shock reflection pattern on the second cylindrical concave reflector is very similar to that observed for higher Mach number, $M_s = 1.6$ with zero initial
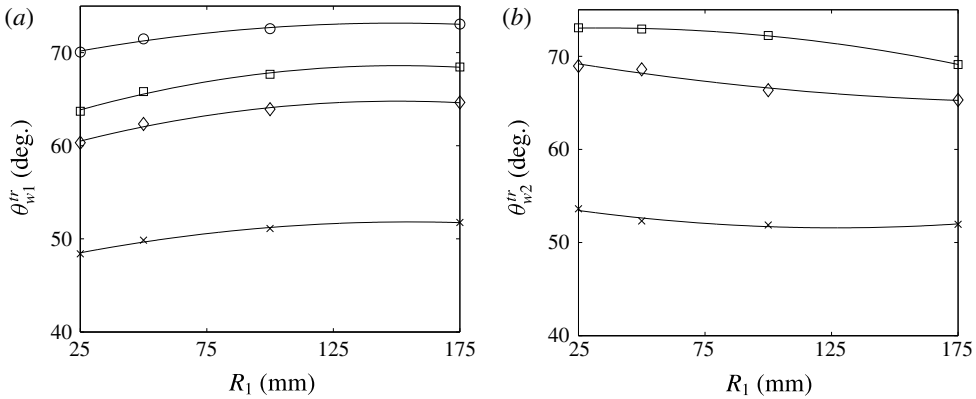
FIGURE 16. InMR $\rightarrow$ TRR transition angle over (*a*) the first; and (*b*) the second cylindrical concave reflector. By varying the radius, $R_1$ while keeping $R_2 = 50$ mm for different incident-shock-wave Mach numbers, $\bigcirc$- $M_s = 2.5$, $\square$- $M_s = 1.9$, $\diamondsuit$ $M_s = 1.6$, $\times$-$M_s = 1.2$.

wedge angle and $R_1 = R_2 = 50$ mm. This is noticed consistently for all other $M_s$ with $R_1 = 25$ mm. This behaviour indicates that the additional shock formed during the TRR state on the first reflector reaches quickly the second one, as it has less distance to travel due to the smaller radius.

As $R_1$ increases, the shock reflection structures become closer to those found for $\phi_{w1} = \phi_{w2} = 0°$ and $R_1 = R_2 = 50$ mm. Interestingly, for $M_s = 1.2$, the shock reflection structure on the second cylindrical reflector is similar to that reported in Part I with $M_s = 1.6$, 1.9 and 2.5, and zero initial wedge angle, if the radius, $R_1$ is maintained constant and $\omega_1$ is reduced, or if $R_1$ is reduced while keeping $\omega_1$ constant. Hence, it can be concluded that for various $M_s$, the shock-wave reflection primarily depends on $\phi_{w1}$, $R_1$ and $\omega_1$.

Figure 16(*a,b*) shows the transition angles over both reflectors. As can be seen, the transition on the first one is delayed as $R_1$ is increased. The current results are in contrast with the previous findings of Takayama & Sasaki (1983), in which the InMR $\rightarrow$ TRR transition angle was found to decrease with the increase in the radius of curvature. However, unlike the first reflector, the transition on the second reflector takes place early as the radius is increased.

## 5. Summary

Shock-wave reflections over double-concave cylindrical reflectors have been investigated. Numerical simulations were carried out to study the changes in the reflected wave structure with regards to the geometrical parameters of the reflectors as well as the incident-shock-wave Mach number. The results reveal several interesting shock reflection behaviours starting from the conventional irregular reflection to regular reflection transitions on the first cylindrical reflector to the TP merging of on the second. For the first time, a single-TP $\rightarrow$ double-TP $\rightarrow$ single-TP $\rightarrow$ double-TP transition has been observed on the same reflector. Moreover, for the same wedge reflector, the flow features exhibit strong differences in shock-wave reflection patterns over the first and the second reflectors. Additionally, it is noticed that the shock reflection over the second reflector varies considerably depending on how quickly

the diffracted shock reaches the incident wave. The geometrical factors essentially responsible for this behaviour are $\phi_{w1}$, $R_1$ and $\omega_1$, and the combination of the latter parameters determines the distance travelled by the diffracted shock wave, $d'$. In addition, contrary to past studies where SMR $\rightarrow$ TMR $\rightarrow$ DMR transition process has been observed, an SMR $\rightarrow$ DMR $\rightarrow$ TMR transition process is observed in the present study for the first time.

## Acknowledgements

## REFERENCES

BEN-DOR, G. 1980 Analytical solution of double-Mach reflection. *AIAA J.* **18**, 1036–1043.

BEN-DOR, G. 1987 A reconsideration of the three-shock theory for a pseudo-steady Mach reflection. *J. Fluid Mech.* **181**, 467–484.

BEN-DOR, G. 2007 *Shock Wave Reflection Phenomena*, 2nd edn. Springer.

BEN-DOR, G., DEWEY, J. M. & TAKAYAMA, K. 1987 The reflection of a plane shock wave over a double wedge. *J. Fluid Mech.* **176**, 483–520.

BEN-DOR, G. & ELPERIN, T. 1991 Analysis of the wave configuration resulting from the termination of an inverse Mach reflection. *Shock Waves* **1** (3), 237–241.

BEN-DOR, G. & GLASS, I. I. 1979 Domains and boundaries of non-stationary oblique shock-wave reflexions. Part 1. Diatomic gas. *J. Fluid Mech.* **92**, 459–496.

BEN-DOR, G. & TAKAYAMA, K. 1985 Analytical prediction of the transition from Mach to regular reflection over cylindrical concave wedges. *J. Fluid Mech.* **158**, 365–380.

BEN-DOR, G., TAKAYAMA, K. & KAWAUCHI, T. 1980 The transition from regular to Mach reflexion and from Mach to regular reflexion in truly non-stationary flows. *J. Fluid Mech.* **100**, 147–160.

BRYSON, A. E. & GROSS, R. W. F. 1961 Diffraction of strong shocks by cones, cylinders, and spheres. *J. Fluid Mech.* **10**, 1–16.

CHAUDHURI, A., HADJADJ, A. & CHINNAYYA, A. 2011a On the use of immersed boundary methods for shock/obstacle interactions. *J. Comput. Phys.* **230** (5), 1731–1748.

CHAUDHURI, A., HADJADJ, A., CHINNAYYA, A. & PALERM, S. 2011b Numerical study of compressible mixing layers using high-order WENO schemes. *J. Sci. Comput.* **47**, 170–197.

COLELLA, P. & GLAZ, H. M. 1984 Numerical calculation of complex shock reflections in gases. In *4th Mach Reflection Symposium*, pp. 154–158. Sendai.

DRIKAKIS, D., OFENGEIM, D., TIMOFEEV, E. & VOIONOVICH, P. 1997 Computation of non-stationary shock-wave/cylinder interaction using adaptive-grid methods. *J. Fluids Struct.* **11** (6), 665–692.

GEVA, M., RAM, O. & SADOT, O. 2013 The non-stationary hysteresis phenomenon in shock wave reflections. *J. Fluid Mech.* **732**, R1.

GRUBER, S. 2012 Weak shock wave reflections from concave curved surfaces. MSc thesis, University of Witwatersrand, South Africa.

GVOZDEVA, L. G., LAGUTOV, YU. P. & FOKEEV, V. P. 1982 Transition from mach reflection to regular reflection when strong shock waves interact with cylindrical surfaces. *Fluid Dyn.* **17** (2), 273–278.

HADJADJ, A. & KUDRYAVTSEV, A. 2005 Computation and flow visualization in high-speed aerodynamics. *J. Turbul.* **6**, 1–25.

HEILIG, W. H. 1969 Diffraction of a shock wave by a cylinder. *Phys. Fluids* **12** (5), I154–I157.

HENDERSON, L. F. & LOZZI, A. 1975 Experiments on transition of Mach reflexion. *J. Fluid Mech.* **68**, 139–155.

HORNUNG, H. 1986 Regular and Mach reflection of shock waves. *Annu. Rev. Fluid Mech.* **18**, 33–58.

HORNUNG, H. G. & TAYLOR, J. R. 1982 Transition from regular to Mach reflection of shock-waves. Part 1. The effect of viscosity in the pseudosteady case. *J. Fluid Mech.* **123**, 143–153.

ITOH, S., OKAZAKI, N. & ITAYA, M. 1981 On the transition between regular and Mach reflection in truly non-stationary flows. *J. Fluid Mech.* **108**, 383–400.

IZUMI, K., ASO, S. & NISHIDA, M. 1994 Experimental and computational studies focusing processes of shock waves reflected from parabolic reflectors. *Shock Waves* **3** (3), 213–222.

KACA, J. 1988 An interferometric investigation of the diffraction of a planar shock wave over a semicircular cylinder. *UTIAS Technical Note* 269.

KLEINE, H., TIMOFEEV, E., HAKKAKI-FARD, A. & SKEWS, B. W. 2014 The influence of Reynolds number on the triple point trajectories at shock reflection off cylindrical surfaces. *J. Fluid Mech.* **740**, 47–60.

MACH, E. 1878 Über den verlauf von funkenwellen in der ebene und im räume. *Sitz.ber. Akad. Wiss. Wien* **78**, 819–838.

VON NEUMANN, J. 1963 *Collected Works of John von Neumann*, 2nd edn. Pergamon.

RAM, O., GEVA, M. & SADOT, O. 2015 High spatial and temporal resolution study of shock wave reflection over a coupled convex–concave cylindrical surface. *J. Fluid Mech.* **768**, 219–239.

SHADLOO, M. S., HADJADJ, A. & CHAUDHURI, A. 2014 On the onset of postshock flow instabilities over concave surfaces. *Phys. Fluids* **26** (7), 076101.

SKEWS, B. & BLITTERSWIJK, A. 2011 Shock wave reflection off coupled surfaces. *Shock Waves* **21** (6), 491–498.

SKEWS, B. W. & KLEINE, H. 2007 Flow features resulting from shock wave impact on a cylindrical cavity. *J. Fluid Mech.* **580**, 481–493.

SMITH, L. G. 1945 Photographic investigation of the reflection of plane shocks in air *Tech. Rep. OSRD Rep.* 6271. Off. Sci. Res. Dev., Washington DC, USA.

SONI, V., ROUSSEL, O. & HADJADJ, A. 2016 On the accuracy and efficiency of point-value multiresolution algorithms for solving scalar wave and Euler equations. *J. Comput. Appl. Maths*; (under review).

TAKAYAMA, K. & BEN-DOR, G. 1983 A reconsideration of the hysteresis phenomenon in the regular ↔ Mach reflection transition in truly nonstationary flows. *Israel J. Tech.* **21(1/2)**, 197–204.

TAKAYAMA, K. & SASAKI, M. 1983 Effects of radius of curvature and initial angle on the shock transition over concave and convex walls. *Rep. Inst. High-Speed Mech.* **46**, 1–30.

WHITE, D. R. 1951 An experimental survey of the Mach reflection of shock waves. *Tech. Rep.* II–10. Deptartment of Physics, Princeton University, Princeton, USA.

WHITHAM, G. B. 1999 *Linear and Nonlinear Waves*. Wiley.